RSC Advances

PAPER

Hybrid compound based on diethylenetriaminecopper(II) cations and scarce V-monosubstituted β-octamolybdate as water oxidation catalyst†

Halyna I. Buvailo, [ID] [a] Valeriya G. Makhankova, [ID] *[b] Vladimir N. Kokozay,[a] Iryna V. Omelchenko, [ID] [c] Svitlana V. Shishkina, [ID] [c] Alina Bieńko, [ID] [d] Mariia V. Pavliuk[e] and Sergii I. Shylin [ID] *[e]

Herein, we report on a new hybrid compound $(NH_4)\{[Cu(dien)(H_2O)_2]_2[\beta\text{-}VMo_7O_{26}]\}\cdot1.5H_2O$ (**1**), where dien = diethylenetriamine, containing an extremely rare mixed-metal pseudo-octamolybdate cluster. An *ex situ* EPR spectroscopy provided insights into the formation of paramagnetic species in reaction mixture and in solution of **1**. The magneto-structural correlations revealed weak antiferromagnetic exchange interactions between the $[Cu(dien)]^{2+}$ cations transmitted by intermolecular pathways. The cyclic voltammetry showed the one-electron process associated with the Cu^{3+}/Cu^{2+} oxidation followed by the multi-electron catalytic wave due to water oxidation with a faradaic yield of 86%. The title compound was thus employed in homogeneous water oxidation catalysis using tris(bipyridine)ruthenium photosensitizer. At pH 8.0, efficiency of the catalytic system attained 0.19 turnovers per second supported by the relatively mild water oxidation overpotential of 0.54 V.

1 Introduction

Polyoxometalates (POMs) are a well-known class of inorganic compounds, which has attracted attention of chemists for years due to their different archetypes, structural flexibilities and functionalities. There have been recently several successful attempts aimed at their decoration with complex cations to obtain hybrid organic–inorganic materials.[1] This strategy may result in formation of products with new promising properties superior to those inherent for the starting building blocks.[2] Another interesting modification of such compounds is a combination of different metal centers in one POM, as for example, in mixed-metal Mo/V anions. It can be used as one of the promising ways to obtain new prospective materials. There is more versatility of Mo-containing polyoxoanion forms

compared to polyoxovanadates, and the former usually have acidic properties. At the same time V-based anions are found to be more active in redox processes.[3,4] Mo/V anions usually have the structural types characteristic for polyoxomolybdates and the introduction of easily-reducible V-centers into a POM may change the nature of products from purely acidic to redox. Moreover, the redox properties can be tuned by the number of V-centers in the clusters.[5] The mixed-metal Mo/V POMs are mainly represented in the literature by the following types of anions: disubstituted α-octamolybdate form $[\alpha\text{-}V_2Mo_6O_{26}]^{6-}$,[6-8] pseudo-Keggin $[Mo_8V_7O_{42}]^{7-}$ and Keggin-based structures $[VMo_{12}O_{40}]^{3-}$, $[VMo_8V_6O_{42}]^{7-}$,[8-10] $[VMo_6O_{22}]^{3-}$ (ref. 11 and 12) and Linqwist $[VMo_5O_{19}]^{3-}$ anion.[13] One the most common Mo/V POM among the mentioned above anions is α-octamolybdate $[\alpha\text{-}V_2Mo_6O_{26}]^{6-}$. Also, a hybrid compound based on the disubstituted β-octamolybdate $[\beta\text{-}V_2Mo_6O_{26}]^{6-}$ and Gd complex has been recently reported.[14]

There were only two publications on a new monosubstituted variant of the β-octamolybdate cluster, $[\beta\text{-}VMo_7O_{26}]^{5-}$. The first compound with this anion was reported in 2018. It consisted of a protonated isoniazid dimer, potassium, sodium cations, $[\beta\text{-}VMo_7O_{26}]^{5-}$ cluster and water molecules.[15] The hybrid had semiconducting properties. Another compound featuring this rare anion was reported in 2019; it was purely inorganic, with the charge of the cluster compensated by potassium cations.[16]

Catalytic properties of POMs have been in a focus of both early studies and the most recent developments of hybrid

[a]*Department of Chemistry, Taras Shevchenko National University of Kyiv, Volodymyrska Street 64/13, 01601 Kyiv, Ukraine*

[b]*Institute of High Technologies, Taras Shevchenko National University of Kyiv, Hlushkova Avenue, 4g, 03022, Kyiv, Ukraine. E-mail: leram@univ.kiev.ua*

[c]*Institute for Single Crystals, National Academy of Sciences of Ukraine, Nauky Ave 60, 61001 Kharkiv, Ukraine*

[d]*Faculty of Chemistry, University of Wroclaw, F. Joliot-Curie 14, 50-383 Wroclaw, Poland*

[e]*Department of Chemistry – Ångström Laboratory, Uppsala University, P. O. Box 523, 75120 Uppsala, Sweden. E-mail: sergii.shylin@kemi.uu.se*

† Electronic supplementary information (ESI) available. CCDC 1958821. For ESI and crystallographic data in CIF or other electronic format see DOI: 10.1039/d1ra05030c

organic–inorganic materials.[17] Compared to molecular catalysts, POMs have distinctive properties as, for example, tunable acidity and rich redox chemistry, inherent resistance to oxidative decomposition, high thermal stability, and possibility for photosensitization.[18] Large-scale industrial applications of POMs include alkenes hydration[19] and oxidation,[20] ketones amination,[21] and esterification processes.[22] The applications of POM-based materials to solar fuels production, is becoming a new strategy in the field of artificial photosynthesis. Various POMs have been examined in different functional roles for solar fuel generation, including photosensitizers, catalysts and charge transfer relays.[23–27]

This paper is a continuation of our research devoted for the synthesis of hybrid compounds based on POMs under mild conditions.[3,4,28–30] Our work is focused on the study of influence of synthetic conditions such as the stoichiometry of reagent, metal sources in the reaction mixtures and the time of interaction. Previously we have successfully synthesized organic–inorganic hybrid compounds with Mo/V anions based on mixed-metal α-octamolybdate $[\alpha\text{-}V_2Mo_6O_{26}]^{6-}$ and Keggin $[PMo_8V_4O_{40}]^{7-}$ anions.[28,30] Herein, we report new compound $(NH_4)\{[Cu(dien)(H_2O)_2]_2[\beta\text{-}VMo_7O_{26}]\}\cdot 1.5H_2O$ (1) based on monosubstituted β-octamolybdate anion. The obtained 1 is a first example of compound based on extremely rare $[\beta\text{-}VMo_7O_{26}]^{7-}$ anion with Cu-containing complex cations.

2 Experimental

2.1 Synthesis of $(NH_4)\{[Cu(dien)(H_2O)_2]_2[\beta\text{-}VMo_7O_{26}]\}\cdot 1.5H_2O$ (1)

All reagents were of analytical grade and used as purchased without further purification. The mixture of Cu powder (0.025 g, 0.40 mmol), $VOSO_4$ (0.239 g, 1.20 mmol) and $(NH_4)_6$-$Mo_7O_{24}\cdot 4H_2O$ (0.847 g, 0.685 mmol) was placed in 50 mL conical flask and 15 mL of water was poured into the solid reagents. Diethylenetriamine (dien, 0.043 mL, 0.40 mmol) was then added under vigorous stirring. The reaction mixture was mechanically stirred at 60–65 °C in open system with air access for 2.5 h and total dissolution of metal powder was observed. The resulting hot solution was filtered and cooled down to the room temperature. Slow evaporation of the filtrate (pH = 4.98) yielded blue crystals of 1 in a day. Yield 0.15 g (47% by copper). Anal. Calc./found for $Cu_2VMo_7O_{31,5}C_8N_7H_{41}$: C – 6.05/6.22; H – 2.60/2.24; N – 6.17/6.00%.

2.2 Crystallography

Single crystal diffraction data was obtained on an Xcalibur-3 diffractometer using Mo-Kα radiation ($\lambda = 0.71073$ Å) at 298 K. Empirical absorption correction was provided with a multiscan method using spherical harmonics, implemented in the SCALE3 ABSPACK scaling algorithm of the CrysAlisPro program package.[31] Structure was solved by direct methods and refined against F^2 within anisotropic approximation for all non-hydrogen atoms using the OLEX2 (ref. 32) program package with SHELXT and SHELXL modules.[33,34] All H atoms were placed in idealized positions (C–H = 0.97 Å, N–H = 0.85–0.89 Å,

O–H = 0.84–0.91 Å) and constrained to ride on their parent atoms, with $U_{iso} = 1.2$ Ueq. (except $U_{iso} = 1.5$ Ueq. for hydroxyl groups). Final refinement was converged at $R_1 = 0.0573$, w$R^2 = 0.1721$, GOF = 1.054. Atom coordinates and crystallographic parameters have been deposited to the Cambridge Crystallographic Data Centre (CCDC 1958821).

2.3 Magnetic susceptibility measurements

The DC magnetic susceptibility was recorded using the SQUID magnetometer (MPMS, Quantum Design) calibrated with a palladium rod (Materials Research Corporation, purity 99.9985%). The crystalline sample (ca. 11 mg) was powdered in order to prevent its displacement in the magnetic field. The susceptibility data was acquired at the field of 0.5 T in the temperature range from 1.8 to 300 K. The susceptibility was corrected in respect to the background signals and underlying diamagnetism and transformed to the effective magnetic moment. The field-dependent magnetization measurements were carried out at $T = 2.0$ K in the magnetic field range up to 5 T. No remnant magnetization was detected.

2.4 Water oxidation studies

Water oxidation experiments were carried out in a 1.5 mL cuvette containing 1.0 mL of the aqueous catalytic mixture. The content of the mixture was as follows: 4 μM of the title complex, 0.1 mM of $\{[Ru(bpy)_3](ClO_4)_2\}\cdot 6H_2O$, 2 mM of $Na_2S_2O_8$ in borate buffer (0.04 M, pH = 8.0). In the reference experiment, 8 μM solution of $CuCl_2\cdot 2H_2O$ or $[Cu(dien)](ClO_4)_2$ were used instead of the title complex with other components being in identical quantities. Oxygen evolution was detected polarographically by using a Clark-type electrode separated from the catalytic mixture by a Teflon membrane. Air-saturated distilled water ($[O_2]_{20\,°C} = 276$ μm) was used for calibration of the electrode. The cell was purged with argon gas before each experiment, and the solution in the cell was continuously stirred. Blue light LEDs ($\lambda = 450$ nm, 3 W) were used as illumination sources. The TOF and TON were calculated based on the total number of copper centres in compounds. TOF = number of O_2 molecules evolved per second per one Cu ion at the maximum rate of oxygen evolution ($mol_{(O2)}\,mol_{(Cu)}^{-1}\,s^{-1}$); TON = total number of O_2 molecules per one Cu atom evolved by the moment of time, when reaction rate decreased to zero ($mol_{(O2)}\,mol_{(Cu)}^{-1}$). All experiments were repeated three times to obtain reproducible TON and TOF values.

2.5 Electrochemistry

Cyclic voltammograms were recorded using an electrochemical three-electrode cell with a 3 mm glass carbon working electrode, a glassy carbon rod counter electrode, and an Ag/AgCl in saturated KCl aqueous solution reference electrode ($E = +0.195$ vs. NHE). The counter and reference electrodes were in compartments separated from the bulk solution by fritted discs. The working electrode was polished with 0.05 μm alumina paste and sonicated before use. The solution under study (5 mL) contained the title complex (0.25 mM), borate buffer (0.04 M, pH 8.0) and $KClO_4$ (0.1 M) as a supporting electrolyte. Before all measurements, oxygen was removed from the cell by bubbling

argon through the stirred solutions. Samples were kept under argon during the measurements. Controlled potential electrolysis experiments were carried out in a three-electrode cell (ITO glass working electrode, Pt counter electrode and a miniature Ag/AgCl reference electrode) equipped with a Clark-type electrode for dissolved oxygen measurements.

2.6 Other methods

CHN analysis was performed using a Vario El Cube elemental analyzer. Infrared (IR) spectrum was recorded in the range of 400–4000 cm^{-1} in KBr pellets using a PerkinElmer Spectrum BX spectrometer. The EPR spectra were recorded on Bruker ELEXSYS E500 CW-EPR spectrometer operating at X-band equipped with frequency counter and NMR Teslameter.

3 Results and discussion

Hybrid compound based on mixed-metal Mo/V polyoxoanion was obtained from reaction system Cu^0 – dien – $(NH_4)_6Mo_7O_{24}$ – $VOSO_4$ – H_2O in the course of the one-pot synthesis accompanied by air oxidation. In contrast to previously studied system with V_2O_5 as a source of vanadium,[28] this procedure yielded another type of POM, namely, the rare mixed-metal $[\beta\text{-}VMo_7O_{26}]^{5-}$ anion. The advantage of the use of metallic Cu as the source of Cu cations is the anion deficiency conditions during the synthesis resulting in the formation and crystallization of hybrid compound with negatively charged POM.

Compound **1** has cationic–anionic structure containing two complex cations $[Cu(dien)(H_2O)_2]^{2+}$, ammonium, and V-substituted $[\beta\text{-}VMo_7O_{26}]^{5-}$ polyoxoanion (Fig. 1); the crystal

Fig. 1 Mixed polyhedral and ball-and-stick representation of the structure of **1** (a) and chains parallel to (100) direction in **1** (b). Color code: Cu, cyan, Mo yellow, V orange, O grey, N blue, C black. All of the hydrogen atoms and crystallization water molecules are omitted for clarity. Hydrogen bonds are shown as dashed lines.

also contains crystallization water molecules. The POM is based on a common β-octamolybdate structure type, however, one of the Mo centers is substituted by V. All metal centers (V and Mo) have distorted octahedral oxygen surrounding. The most distorted are coordination polyhedra at the Mo(1)/V(1) centers (M–O bond lengths vary in the range of 1.651–2.396, while all other polyhedra possess the range of 1.699–2.326 Å). Generally the geometrical parameters for the anion are close to those published previously.[15,16] The coordination polyhedron of Cu^{II} center is formed by three nitrogen atoms from the dien molecule and two oxygen atoms from the coordinated H_2O. The value of the angular structural index parameter τ is 0.21 $[\tau = (\beta - \alpha)/60°$, α and β are the two largest valence angles centred on the same Cu atom, $\alpha < \beta]$.[35] Thus, the $[CuN_3O_2]$ coordination polyhedron has distorted square-based pyramidal geometry.

In the crystal, complex anions alternate with ammonium forming chains along the (100) crystallographic direction by the means of charge-assisted N–H···O′ hydrogen bonds. Each complex cation is linked to the one of the POM anions by N–H···O′ and O–H···O′ hydrogen bonds involving the hydrogen atoms from dien and water ligands. Interactions of the complex cations with POM anions from other chains are rather weak. Chains are linked *via* the bridging coordinated water molecules that connect the amino group of the dien ligand of the cation from one chain with the water ligand of the cation from a neighboring chain, forming the network.

The IR spectrum of **1** (Fig. S1, ESI†) is different from a typical one for non-substituted β-octamolybdate anion,[36,37] but has a similar pattern with other compounds based on $[\beta\text{-}VMo_7O_{26}]^{5-}$.[15,16] The most intensive bands at 930, 900 and 870 cm^{-1} are assigned to M = O stretching (M = Mo, V), while the bands at the region 850–470 cm^{-1} correspond to asymmetric and symmetric deformation vibrations of the M–O–Mo bonds. The characteristic bands attributed to water molecules (O–H) and coordinated dien ligands (N–H) are in the 3500–2800 cm^{-1} region.[28]

In order to understand the paramagnetic species transformation in the synthesis of **1**, we compare EPR spectra of the reaction mixture obtained after dissolution of metallic copper with the aqueous solution of as-prepared **1**. Two types of paramagnetic species in the frozen filtrate of reaction mixture (Sol1 in Fig. 2) were determined by EPR spectroscopy in the current system.

The spin-Hamiltonian parameters determined by the simulation of the experimental spectrum are as follows: $g_\parallel = 2.230$, $A_\parallel = 194 \times 10^{-4}$ cm^{-1} and $g_\parallel = 2.410$, $A_\parallel = 138 \times 10^{-4}$ cm^{-1}. The values are in agreement with those reported previously for Cu(II) complexes with N4 and O4 atoms in an equatorial plane, respectively.[38] The additional weak lines observed in the spectrum at the high magnetic field were assigned to the hyperfine splitting of parallel orientation of oxovanadium(IV) species indicating that insignificant quantities of V(IV) remained after the interaction. In contrast, the EPR spectrum of the aqueous solution of crystals of **1** revealed only one type of copper centers with $g_\parallel = 2.232$, $A_\parallel = 183 \times 10^{-4}$ cm^{-1} that is in accordance with N3O equatorial surrounding of metal ions (Sol cryst **1** in Fig. 2). The difference between Sol1 and Sol cryst **1** indicated the
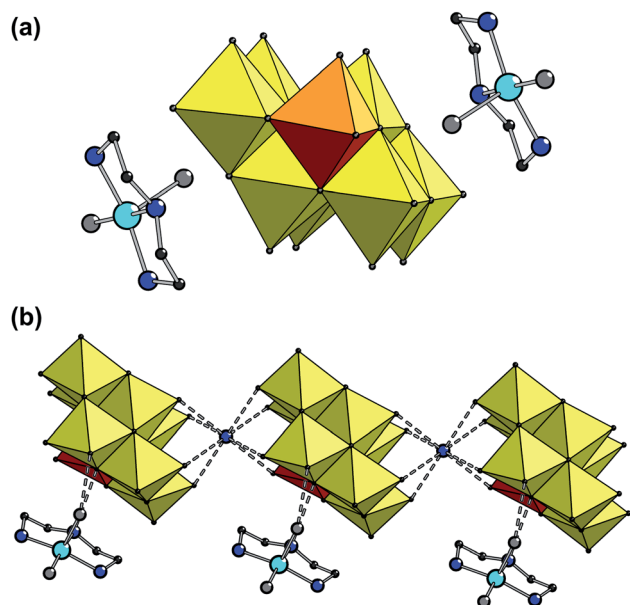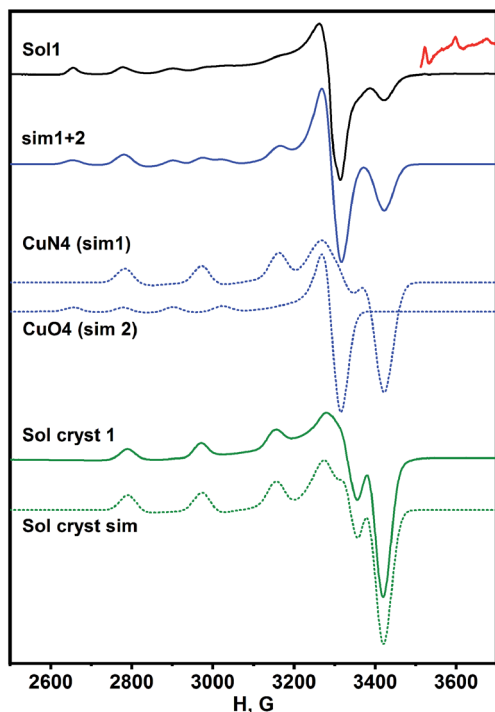
Fig. 2 EPR spectra of frozen aqueous solutions (77 K) of the reaction mixture (Sol1), the title compound (Sol cryst **1**), and the corresponding simulated spectra for the copper(II) species with the EPR parameters given in the text. The fragment of the magnified spectrum of Sol1 featuring V(IV) is shown in red.

Fig. 3 DC magnetic data for **1**. (a) Temperature dependence of χ_M (half-open circles) and $\chi_M T$ (open circles). (b) Dependence of the magnetic moment on the external magnetic field. The solid lines on both graphs are calculated using the HDVV spin Hamiltonian and PHI program.[39]

rearrangement of complex units during crystallization. Thus, similar copper cationic complexes exist in the solid state and in the aqueous solution of **1**. There was no residual V(IV) found in the solution of **1**.

The magnetic properties of **1** recorded in the temperature range 1.8–300 K are shown in Fig. 3. The product of the molar magnetic susceptibility with temperature, $\chi_M T$ (and the effective magnetic moment) slowly decreases on cooling from room temperature down to 40 K; $\chi_M T$ (300 K) = 1.00 cm^3 mol^{-1} K (μ_{eff} = 2.83 μ_B) is adequate to expected for two Cu(II) ions ($S = \frac{1}{2}$ each) without any exchange interactions with g_{av} = 2.00.

A rapid decrease of the $\chi_M T$ below 40 K is observed down to 0.43 cm^3 mol^{-1} K at 1.8 K. The susceptibility behavior indicates antiferromagnetic exchange interactions between the copper ions in **1**. As a local maximum of the $\chi_M T(T)$ function is not seen in the temperature range 1.8–300 K, the magnitude of such interaction is rather small.[40]

The exchange interaction between two Cu(II) ions ($S_A = S_B = \frac{1}{2}$) in the title compound was described by the model of binuclear units realized through Cu$\cdots$Cu intermolecular contacts. The calculations were based on the Heisenberg–Dirac–Van Vleck Hamiltonian in zero field given by eqn (1). The temperature independent paramagnetism (TIP) and the fraction of paramagnetic impurities (x) were also included into the fitting procedure.

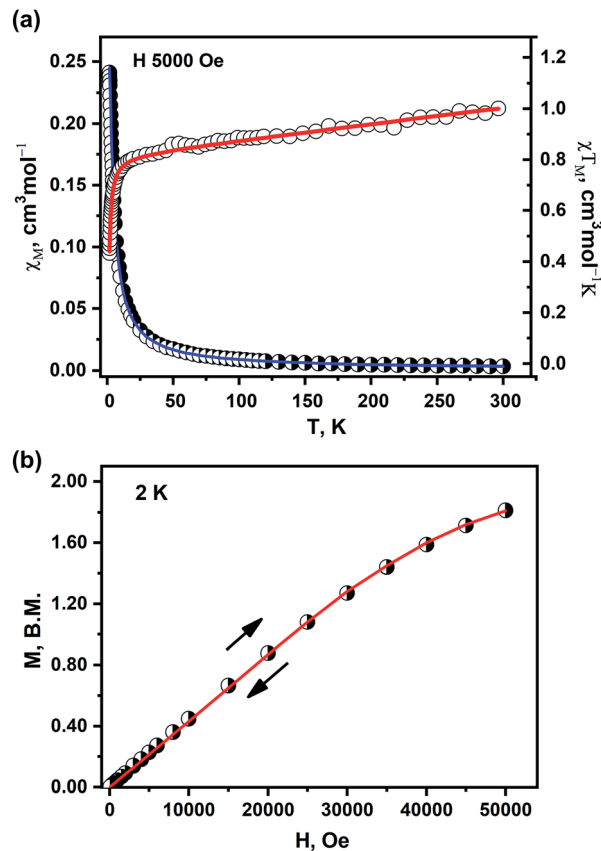$$\hat{H} = -J\hat{S}_A\hat{S}_B \langle S_z \rangle \, \hat{S}_z \qquad (1)$$

The best agreement with the experimental magnetic data for **1** was obtained with the magnetic exchange parameter $J = -0.93$ cm^{-1}, $g = 2.09$, and $x = 0.005$, TIP = 334×10^{-6} cm^3 mol^{-1}, $R = \Sigma[(\chi T)\exp - (\chi T)\text{calc.}]^2/\Sigma[(\chi T)\exp]^2 = 7.1 \times 10^{-5}$ (red and blue lines in Fig. 3a). The value of the J parameter confirms that the exchange interaction between the nearest Cu(II) centers in the examined complex is antiferromagnetic in nature but weak and can be attributed to the presence of the superexchange pathway through the long Cu$\cdots$Cu contacts.
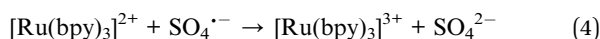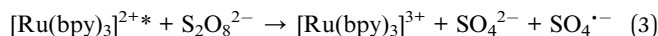
Detailed examination of the crystal packing of the complex **1** suggests that such weak magnetic coupling may be transmitted through double nonbonding Cu–O$\cdots$O–Cu contact with distance $d = 4.265$ Å or 5.860 Å and angle of $97.8°$ or $94.7°$ (far from the optimal angle $180°$ typical for strong interaction)[41,42] with the alternating Cu–Cu separations of 6.059 Å and 6.944 Å. (Fig. S2, ESI†). Additionally, the magnetic interactions through a longer Cu$\cdots$Cu distance (7.682 Å) can be supported by N–H$\cdots$O' and O–H$\cdots$O' hydrogen bonds involving the hydrogen atoms from dien and water ligands.

The magnetization *vs.* field dependence recorded and 2.0 K did not reach a saturation plateau (Fig. 3b). In such case, the ground state has $S = 1$ and the magnetization per a formal Cu$_2$ unit should saturate to the value of 2.0 μ_B at field above 5 T.

The catalytic activity of the title compound in water oxidation was evaluated using tris(bipyridine)ruthenium(II) light harvester and sodium persulfate as a sacrificial electron acceptor (Fig. S3, ESI†).[43,44] The water-based catalytic mixture buffered by H_3BO_3–NaOH (pH 8.0) was driven by the visible light (3 W LEDs, $\lambda = 450$ nm) to excite the photosensitizer:

$$[Ru(bpy)_3]^{2+} + h\nu \rightarrow [Ru(bpy)_3]^{2+*} \qquad (2)$$
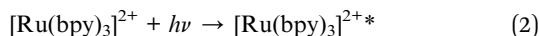
The excited triplet state of the photosensitizer is rapidly quenched by persulfate giving $[Ru(bpy)_3]^{3+}$ and sulfate radical (eqn (3)), which then reacts with the second equivalent of the light harvester:

$$[Ru(bpy)_3]^{2+*} + S_2O_8^{2-} \rightarrow [Ru(bpy)_3]^{3+} + SO_4^{2-} + SO_4^{\cdot -} \qquad (3)$$

$$[Ru(bpy)_3]^{2+} + SO_4^{\cdot -} \rightarrow [Ru(bpy)_3]^{3+} + SO_4^{2-} \qquad (4)$$

The photochemical generation of $[Ru(bpy)_3]^{3+}$ can be observed by steady-state UV-vis spectroscopy (Fig. S4, ESI†). When the copper complex is present in the reaction mixture, no accumulation of $[Ru(bpy)_3]^{3+}$ is observed because of the fast hole transfer to the catalyst with the subsequent oxidation of water. Using the Clark-type electrode, we have observed oxygen evolution with turnover number (TON, number of O_2 molecules evolved per one copper atom) of 10 and turnover frequency (TOF) of 0.19 s^{-1} (Fig. 4). Thus, the catalytic activity of the title complex is similar to that reported for Cu-containing catalysts with $[\alpha\text{-}V_2Mo_6O_{26}]$ (POM).[28] Importantly, efficiency of the title complex is considerably higher compared to the plane Cu^{2+} salt under virtually identical photocatalytic conditions. For $CuCl_2$ used as a catalyst, we were able to observe $\sim$2.5 O_2 molecules produced per one copper.

However, when a $[Cu(dien)]^{2+}$ complex was used as a catalyst, the catalytic system reached the TON of 6 (green trace in Fig. 4),
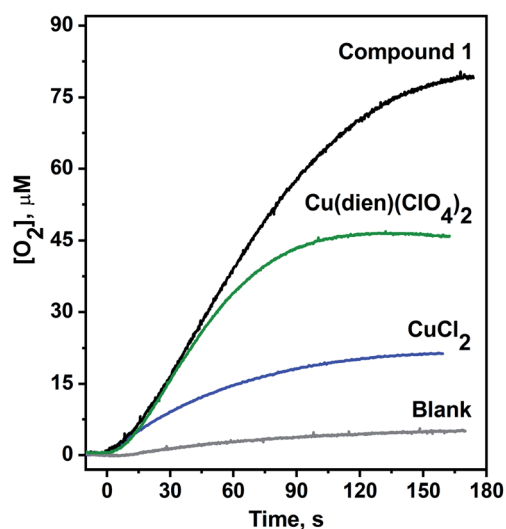

Fig. 4 Oxygen evolution traces obtained for the title complex (4 μM, black curve), [Cu(dien)](ClO$_4$)$_2$ (8 μM, green curve) and CuCl$_2$ (8 μM, blue curve) at pH 8.0. Oxygen evolution in the absence of any copper is shown in gray. Zero on the timescale corresponds to the start of illumination with LEDs (450 nm).
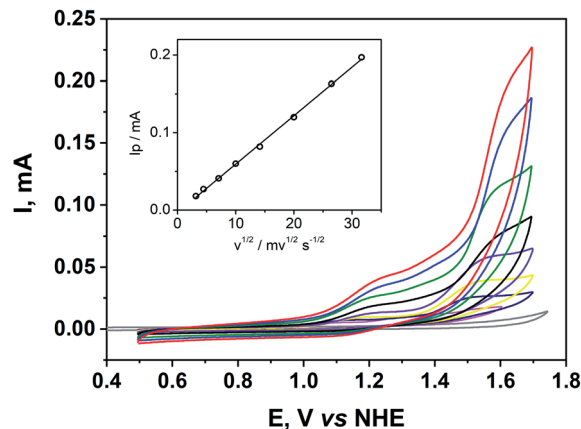

Fig. 5 Cyclic voltammograms for the title complex recorded at different scan rates between 10 mV s^{-1} (magenta) and 1000 mV s^{-1} (red) at pH 8.0. The background current recorded at 100 mV s^{-1} is shown in gray. Inset shows dependence of the peak current at 1.6 V vs. NHE on the square root of the scan rate.

suggesting a pivotal role of the dien ligand in water oxidation catalysis via e.g. stabilization of a presumable Cu^{III} intermediate.[45,46]

The electrochemistry of the title compound was studied in the buffered aqueous solution at pH 8.0 — conditions resembling our photochemical water oxidation experiment. At various scan rates from 10 to 1000 mV s^{-1}, two oxidative waves can be identified (Fig. 5). The first one centered around 1.2 V vs. NHE is the one-electron process that can be assigned to the Cu^{II}/Cu^{III} redox couple.[47] The second wave with onset around 1.3 V is a multi-electron process corresponding to the electrocatalytic water oxidation. Thus, water oxidation using the title compound starts at a relatively mild overpotential 0.54 V compared to other WOCs.[48,49] To understand the role of the ligand environment on the redox chemistry of copper in 1, we recorded cyclic voltammograms for the related complex [Cu(dien)](ClO$_4$)$_2$ (Fig. S5, ESI†). Both compounds exhibit similar oxidation processes up to 1.7 V vs. NHE indicating that the POM fragment in 1 is virtually redox innocent in this potential range. The peak current for the catalytic wave depends linearly on the square root of the scan rate (Fig. 5, inset) indicating a diffusion controlled homogeneous catalysis. The observation rules out a possible contribution of copper oxide precipitate to the catalytic current. Assignment of this oxidation process to the water oxidation was confirmed by controlled potential electrolysis experiments, coupled to oxygen evolution measurements using a Clark-type electrode. When a potential of 1.55 V vs NHE was applied, a stationary current of 0.063 mA was detected with a simultaneous dissolved oxygen increase of 8.5 μM min^{-1}, corresponding to the overall faradaic yield of 86% (Fig. 6). This value indicates that oxidation of the ligand may occur slowly as a side reaction, but not as a dominant redox process at this potential.[45,46]

After 45 min of sustained bulk electrolysis, the working electrode was recovered and immersed in the catalyst-free buffered solution. At the same potential of 1.55 V vs. NHE, the
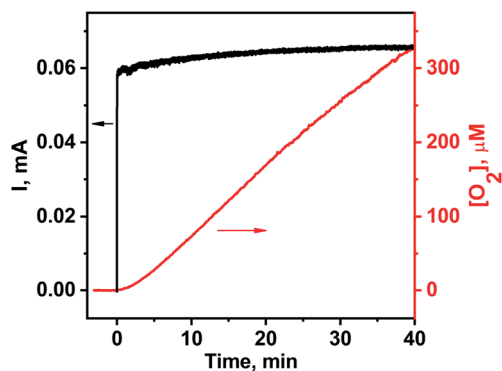
Fig. 6 Electric current (black) and oxygen evolution trace (red) for the bulk electrolysis experiment using the title complex (0.1 mM) at pH 8.0.

initial current of *ca.* 5 mA was observed accompanied by a negligible amount of oxygen evolved (Fig. S6, ESI†), which corroborates the absence of catalytically active precipitates on the working electrode surface.

4 Conclusions

In summary, we report synthesis of a novel hybrid compound based on the extremely rare mixed-metal polyoxoanion [β-VMo_7O_{26}]. The compound was obtained under mild conditions starting from zero-valent copper. The equilibrium of CuN4 and CuO4 species in the reaction mixture was established by EPR spectroscopy, while the solution of the final product **1** contained CuN3O species only. The oxidative process V(IV) → V(V) was almost completed till the end of the interaction while the crystalline **1** contained V solely in its highest oxidation state according to the magnetization studies. The prominent oxidative wave in cyclic voltammograms with onset at 1.3 V *vs.* NHE corresponded to electrocatalytic water oxidation which occurred under diffusion control. The efficiency of the catalytic system with the title compound in homogeneous water oxidation catalysis attained 0.19 turnovers per second supported by the relatively low water oxidation overpotential of 0.54 V.

Conflicts of interest

There are no conflicts to declare.

Acknowledgements

Notes and references

1 D. Li, P. Ma, J. Niu and J. Wang, *Coord. Chem. Rev.*, 2019, **392**, 49–80.

2 N. Lotfian, M. M. Heravi, M. Mirzaei and B. Heidari, *Appl. Organomet. Chem.*, 2019, **33**, e4808.

3 M. V. Pavliuk, E. Mijangos, V. G. Makhankova, V. N. Kokozay, S. Pullen, J. Liu, J. Zhu, S. Styring and A. Thapper, *ChemSusChem*, 2016, **9**, 2957–2966.

4 M. V. Pavliuk, V. G. Makhankova, O. V. Khavryuchenko, V. N. Kokozay, I. V. Omelchenko, O. V. Shishkin and J. Jezierska, *Polyhedron*, 2014, **81**, 597–606.

5 V. F. Odyakov, E. G. Zhizhina, Y. A. Rodikova and L. L. Gogin, *Eur. J. Inorg. Chem.*, 2015, **2015**, 3618–3631.

6 J. Wang, J. Wang, P. Ma and J. Niu, *J. Coord. Chem.*, 2009, **62**, 2641–2647.

7 A.-M. Nenner, *Acta Crystallogr., Sect. C: Cryst. Struct. Commun.*, 1985, **41**, 1703–1707.

8 J. Wang, Y. Feng, J. Zhao, P. Ma, X. Zhang and J. Niu, *J. Coord. Chem.*, 2009, **62**, 3754–3762.

9 L. N. Xiao, Y. Wang, Y. Chen, Y. Peng, G. D. Li, X. B. Cui, S. Y. Shi, T. G. Wang, Z. M. Gao and J. Q. Xu, *Inorg. Chem. Commun.*, 2010, **13**, 1217–1220.

10 L.-M. Duan, C.-L. Pan, J.-Q. Xu, X.-B. Cui, F.-T. Xie and T.-G. Wang, *Eur. J. Inorg. Chem.*, 2003, **2003**, 2578–2581.

11 J. Li, L. Xu, N. Jiang, L. Zhao and F. Li, *Struct. Chem.*, 2011, **22**, 1339–1345.

12 N. Strukan, M. Devcic, B. Kamenar and M. Cindric, *Inorg. Chem. Commun.*, 1999, **2**, 558–560.

13 J. Tucher, Y. Wu, L. C. Nye, I. Ivanovic-Burmazovic, M. M. Khusniyarov and C. Streb, *Dalton Trans.*, 2012, **41**, 9938–9943.

14 Q. Gao, B. Qi, T. Wu and L. Xu, *Inorg. Chem. Commun.*, 2019, **107**, 107481.

15 Y. Zhao, Q. Gao, R. Tao, F. Li, Z. Sun and L. Xu, *Inorg. Chem. Commun.*, 2018, **89**, 94–98.

16 L. Krivosudský, A. Roller and A. Rompel, *Acta Crystallogr., Sect. C: Struct. Chem.*, 2019, **75**, 872–876.

17 S. S. Wang and G. Y. Yang, *Chem. Rev.*, 2015, **115**, 4893–4962.

18 N. I. Gumerova and A. Rompel, *Nat. Rev. Chem.*, 2018, **2**, 0112.

19 Y. Izumi, *Catal. Today*, 1997, **33**, 371–409.

20 K. Sano, H. Uchida and S. Wakabayashi, *Catal. Surv. Asia*, 1999, **3**, 55–60.

21 J. N. Armor, *Appl. Catal., A*, 2001, **222**, 407–426.

22 M. J. Howard, G. J. Sunley, A. D. Poole, R. J. Watt and B. K. Sharma, in *Science and Technology in Catalysis* 1998, ed. H. Hattori and K. Otsuka, Elsevier, 1999, vol. 121, pp. 61–68.

23 J. J. Stracke and R. G. Finke, *ACS Catal.*, 2014, **4**, 79–89.

24 J. Wei, Y. Feng, P. Zhou, Y. Liu, J. Xu, R. Xiang, Y. Ding, C. Zhao, L. Fan and C. Hu, *ChemSusChem*, 2015, **8**, 2630–2634.

25 H. Lv, J. Song, Y. V Geletii, J. W. Vickers, J. M. Sumliner, G. Musaev, P. Kögerler, P. F. Zhuk, J. Bacsa, G. Zhu, C. L. Hill and G. Djamaladdin, *J. Am. Chem. Soc.*, 2014, **136**, 9268–9271.

26 X. B. Han, Y. G. Li, Z. M. Zhang, H. Q. Tan, Y. Lu and E. B. Wang, *J. Am. Chem. Soc.*, 2015, **137**, 5486–5493.

27 Q. Han and Y. Ding, *Dalton Trans.*, 2018, **47**, 8180–8188.

28 H. Buvailo, V. Makhankova, V. Kokozay, I. V. Omelchenko, S. V. Shishkina, J. Jezierska, M. V. Pavliuk and S. I. Shylin, *Inorg. Chem. Front.*, 2019, **6**, 1813–1823.

29 H. I. Buvailo, V. G. Makhankova, V. N. Kokozay, I. V. Omelchenko, S. V. Shishkina, P. Zabierowski, D. Matoga and J. Jezierska, *Eur. J. Inorg. Chem.*, 2017, **2017**, 3525–3532.

30 H. I. Buvailo, V. G. Makhankova, V. N. Kokozay, I. V. Zatovsky, I. V. Omelchenko, S. V. Shishkina, P. Zabierowski, D. Matoga and J. Jezierska, *Eur. J. Inorg. Chem.*, 2016, **2016**, 5456–5466.

31 *CrysAlis PRO*, Agilent Technologies, 2011.

32 O. V. Dolomanov, L. J. Bourhis, R. J. Gildea, J. A. K. Howard and H. Puschmann, *J. Appl. Crystallogr.*, 2009, **42**, 339–341.

33 G. M. Sheldrick, *Acta Crystallogr., Sect. A: Found. Crystallogr.*, 2008, **64**, 112–122.

34 G. M. Sheldrick, *Acta Crystallogr., Sect. C: Struct. Chem.*, 2015, **71**, 3–8.

35 A. W. Addison, T. N. Rao, J. Reedijk, J. van Rijn and G. C. Verschoor, *J. Chem. Soc., Dalton Trans.*, 1984, **9**, 1349–1356.

36 X.-L. Wang, D.-N. Liu, H.-Y. Lin, G.-C. Liu, N. Han, J. Luan and Z.-H. Chang, *RSC Adv.*, 2015, **5**, 56687–56696.

37 A. B. Lysenko, G. A. Senchyk, L. V. Lukashuk, K. V. Domasevitch, M. Handke, J. Lincke, H. Krautscheid, E. B. Rusanov, K. W. Krämer, S. Decurtins and S. X. Liu, *Inorg. Chem.*, 2016, **55**, 239–250.

38 S. Kumar, R. P. Sharma, P. Venugopalan, M. Witwicki and V. Ferretti, *J. Mol. Struct.*, 2016, **1123**, 124–132.

39 N. F. Chilton, R. P. Anderson, L. D. Turner, A. Soncini and K. S. Murray, *J. Comput. Chem.*, 2013, **34**, 1164–1175.

40 G. A. Bain and J. F. Berry, *J. Chem. Educ.*, 2008, **85**, 532.

41 J. L. Wikaira, R. J. Butcher, Ü. Kersen and M. M. Turnbull, *J. Coord. Chem.*, 2016, **69**, 57–71.

42 M. M. Turnbull, C. P. Landee and B. M. Wells, *Coord. Chem. Rev.*, 2005, **249**, 2567–2576.

43 S. I. Shylin, M. V. Pavliuk, L. D'Amario, F. Mamedov, J. Sá, G. Berggren and I. O. Fritsky, *Chem. Commun.*, 2019, **55**, 3335–3338.

44 S. I. Shylin, M. V. Pavliuk, L. D'Amario, I. O. Fritsky and G. Berggren, *Faraday Discuss.*, 2019, **215**, 162–174.

45 C. Lu, J. Du, X.-J. Su, M.-T. Zhang, X. Xu, T. J. Meyer and Z. Chen, *ACS Catal.*, 2016, **6**, 77–83.

46 A. Prevedello, I. Bazzan, N. Dalle Carbonare, A. Giuliani, S. Bhardwaj, C. Africh, C. Cepek, R. Argazzi, M. Bonchio, S. Caramori, M. Robert and A. Sartorel, *Chem.–Asian J.*, 2016, **11**, 1281–1287.

47 M. K. Coggins, M.-T. Zhang, Z. Chen, N. Song and T. J. Meyer, *Angew. Chem., Int. Ed.*, 2014, **53**, 12226–12230.

48 K. J. Fisher, K. L. Materna, B. Q. Mercado, R. H. Crabtree and G. W. Brudvig, *ACS Catal.*, 2017, **7**, 3384–3387.

49 B. Rudshteyn, K. J. Fisher, H. M. C. Lant, K. R. Yang, B. Q. Mercado, G. W. Brudvig, R. H. Crabtree and V. S. Batista, *ACS Catal.*, 2018, **8**, 7952–7960.